Bulgarian Chemical Communications, Volume 58 Issue 2 (pp. 193-199) 2026 DOI: 10.34049/bcc.58.2.NCC03

Quantum chemical insights into porous s-triazine and tri-s-triazine carbon nitrides

J. N. Petkova[1,2], I. Mijakov[1], E. P. Simeonova[1], G. K. Madjarova[1,2]

[1]*Laboratory of Quantum and Computational Chemistry, Faculty of Chemistry and Pharmacy, Sofia University "St. Kliment Ohridski", Sofia, Bulgaria*

[2]*National Centre of Excellence Mechatronics and Clean Technologies, Sofia University "St. Kliment Ohridski", Sofia, Bulgaria*

Received: November 05, 2025; Revised: January 06, 2026

Density functional theory calculations are performed to investigate a series of carbon nitride models based on s-triazine and tri-s-triazine units. Single-pore structures, varying in nanopore shape and size, are extended to form highly porous nanosheets. The structures, electron density distributions, HOMO-LUMO energy gaps are analyzed and compared. Slightly pronounced edge effects indicate possible competition between nanopores during the interactions with gas molecules. This study is an initial step in the quantum chemical investigation of carbon nitride structures for gas mixture separation applications.

Keywords: carbon nitrides, density functional theory, gas separation membranes

INTRODUCTION

Graphene-type carbon nitrides are a class of organic microporous materials that have attracted increasing interest within the scientific community due to their narrow bandwidth, thermal stability, easy synthesis and easy functioning [1-23]. These materials have a wide range of potential applications, including photocatalysis [4], photovoltaic cells [5], sensors [6] and lithium-ion batteries [7]. The naturally stable nanopores make these materials promising candidates for atom-thick membranes for an inexpensive, energy-efficient gas mixture purification and separation. The geometry and electronic structure of the material are crucial factors for all these applications.

Carbon nitrides consist of layers of covalently bonded sp^2-hybridized carbon and nitrogen atoms, primarily based on heptazine and s-triazine units and feature well-defined nanopores [8]. Poly (triazine-imide) (PTI) is an example of s-triazine-based carbon nitride. PTI compounds have a layered 2D π-conjugated planar structure, with triazine fragments linked by imide groups and weak Van der Waals interactions between the individual layers. Another example of carbon nitride, based on s-triazine rings, is g-C_3N_3 material. Unlike PTI, the ring fragments in the g-C_3N_3 are directly linked through covalent bond between carbon atoms. A 2D π-conjugated plane is also formed, but the shape and the size of the pores are differing from those of the PTI.

Another class of graphite-like carbon nitrides are with stoichiometry C_3N_4. g-C_3N_4 exists in two types: one based on triazine unit (TGCN) and another based on heptazine fragments (HGCN). TGCN contains three triazine fragments linked by amine groups, resulting in much smaller nanopores in comparison to PTI and C_3N_3. The most studied theoretically and experimentally carbon nitride is HGCN with three heptazine units. Two forms of HGCN are identified – amorphous and crystalline [9]. The amorphous form shows weaker photocatalytic activity, but is characterized by a smaller band gap width. Kang and co-authors propose a method for synthesis of amorphous form with a band gap energy of 1.9 eV. Quantum chemical calculations indicated that the folded form of HGCN has lower energy than the planar structure due to the reduction of repulsion between the lone pairs of nitrogen atoms [10].

Different theoretical and experimental approaches are used to study the application of the PTI, C_3N_3, TGCN and HGCN carbon nitrides as gas separation membranes [11-17] and as photocatalysis [18, 19]. The adsorption properties, selectivity and permeability are evaluated. The electronic structure and band gap are discussed. However, to the best of our knowledge, there is no systematic investigation conducted under consistent conditions, models, and computational parameters on different types of carbon nitride. Such a study would allow a comparison of the carbon nitride characteristics and provide a basis for developing a model to obtain materials with the desired properties.

* To whom all correspondence should be sent:
Email: *fhjp@chem.uni-sofia.bg*

The current quantum chemical study aims to systematically evaluate and compare the structures and electronic properties of four distinct carbon nitrides - PTI, C_3N_3, TGCN and HGCN, with a particular emphasis on the nanopore characteristics. Geometry, electron density distribution, and the HOMO-LUMO gap - characteristics related to the sieving, adsorption, and permeability capacities of the nanopores - are discussed. The influence of the model size was also assessed and analyzed. These findings provide a foundation for investigating the potential of PTI, C_3N_3, TGCN and HGCN as atom-thick membranes for gas mixtures separation.

Computational details

Four types of carbon nitrides were investigated in the study (Figure 1). Three of them – PTI, C_3N_3 and TGCN - are based on s-triazine units. In PTI and TGCN, the s-triazine units are linked *via* nitrogen groups, whereas in C_3N_3, the s-triazine fragments are directly bound through carbon–carbon bonds between the rings. The results for the triazine-based carbon nitrides were compared with those for HGCN, where tri-s-triazine units are linked by amine groups. The four carbon nitrides contain nanopores of varying shapes and sizes: C_3N_3 has spherical pores, PTI and TGCN feature triangular pores, and HGCN has hexagonal pores. Nanopore size was determined by measuring the maximum distance between atoms in the pore's interior (Figure 1). The smallest is the nanopore of TGCN (~2.6 Å), followed by PTI (~ 4.05 Å), HGCN (~ 4.90 – 5.00 Å), and the largest one is in C_3N_3 (~ 5.47 Å).

All calculations were performed with the B3LYP hybrid functional with added three-parameter empirical correction (GD3) [20]. The 6-31G** basis set was used. The electron density distribution was estimated by Natural Population Analysis (NPA), which is a component of the Natural Bond Orbital (NBO) analysis method [21]. The calculations were carried out with Gaussian software [22].

RESULTS AND DISCUSSION

Structure of PTI, C_3N_3, TGCN and HGCN

In PTI, the nanopores are formed from six s-triazine fragments that are linked by nitrogen groups. The interior of the nanopores is defined by the presence of alternating sp^2- carbon and sp^2-, sp^3-nitrogen atoms (Figure 1). The nitrogen groups play a key role in determining the triangular shape of the nanopore, with hydrogen atoms oriented towards the interior. The distance between these hydrogen atoms is approximately 4.05 Å (Figure 1). The lengths of the C-N bonds in the s-triazine rings are in the range of 1.329 to 1.353 Å. The longest bonds are those with the nitrogen linker (1.379÷1.380 Å). Both the model featuring a single nanopore and the 2D nanosheet with ten pores (*10*-PTI) have a fully planar structure, with pores of identical size (Figure 2). The enlargement of the model does not result in any significant structural changes.

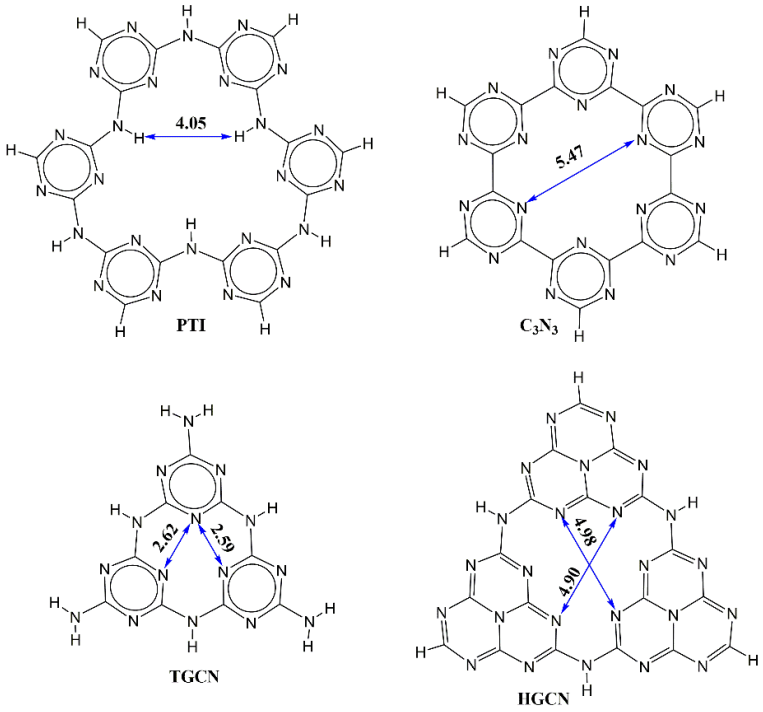

Figure 1. Chemical structures of PTI, C_3N_3, TGCN and HGCN containing a single nanopore. The sizes of the nanopores are indicated.

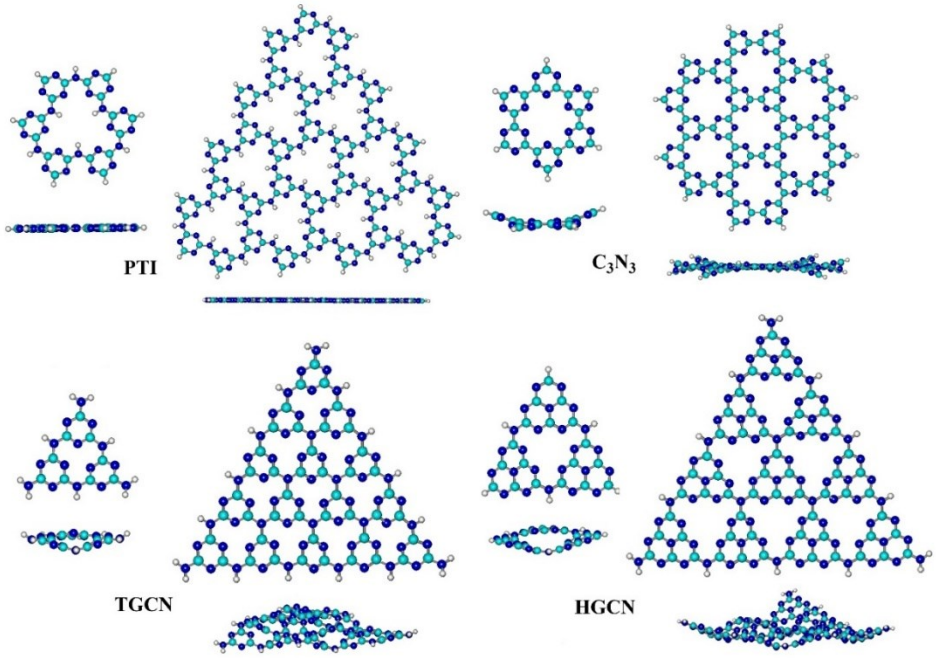

Figure 2. Front and side views of the smallest and largest structures of the modelled carbon nitrides (C green, N – blue, H - grey). Structure optimization is performed with B3LYP-D3/6-31G**.

In contrast to PTI, C_3N_3 is constructed from s-triazine rings directly linked by C-C bonds (Figure 1). As a result, the molecule is not quite planar. A distortion occurs due to the slight rotations (about 20°) around four of the C–C bonds in the pore. This causes two of the opposing triazine rings to tilt upwards, while the other four tilt downwards (Figure. 2). The pore size, defined by circumscribed circle formed by the imine nitrogen atoms in the interior of the nanopore, is with diameter (the longest distance measured between each pair of opposite nitrogen) of 5.47 Å (Figure 1). The carbon-nitrogen bond lengths vary between 1.335 and 1.339 Å, the length of the carbon-carbon bond is about 1.504-1.506 Å. The 2D nanosheet of C_3N_3 with seven pores (*7*-C_3N_3) is characterized by folding at the outer pores and flattening of the inner pores. The deformation in the periphery of the nanosheet is about 13÷23° (similar to the distortion in the single C_3N_3 pore) while the inner pore remains relatively planar, with an out-of-plane deviation of about 2.5÷3°.

The optimized structure of the single-pore model of TGCN is presented in Figure 2. The interior of the nanopore is defined by three imine nitrogen atoms, one from each ring. To minimize repulsion between the lone electron pairs of these nitrogen atoms, the three-ring framework becomes distorted, resulting in a nonplanar stable structure for TGCN (Figure 2). Two of the three nitrogen atoms lie in the same plane, separated by 2.59 Å, while the third nitrogen atom is displaced from this plane by 39° at a distance of 2.62 Å. The pore adopts a nonplanar, open-ring geometry (Figure 2). In the 2D TGCN nanosheet containing ten nanopores (*10*-TGCN), this bent structure is preserved (Figure 2). The central nanopore is characterized with additional distortion compared to the single-pore model and shows slightly greater deformation than the other pores in the nanosheet. The dihedral angle between the two nitrogen atoms, that remain coplanar in the smallest model, is ~18° (5 - 13° in different cavities). The other dihedral angles describing the mutual nonplanarity of the nitrogen atoms are 40° and -57° (30° - 55° across the different pores). The three nitrogens from the pore lie in distinct symmetry planes, with interatomic distance of approximately ~2.5 - 2.8 Å, slightly longer than those in the single-pore TGCN model.

The single-pore HGCN structure is composed of three tri-s-triazine fragments linked by amino groups (Figure 1). HGCN has a bent geometry similar to this of TGCN. One of the heptazine fragments deviates with 43° from the plane formed by the other, indicating a slightly larger distortion compared to TGCN. HGCN forms an open nanopore similar in shape to that of TGCN, but with a larger size. The maximum distance between nitrogen atoms from opposite rings is ~4.98 Å. The bent geometry becomes more pronounced in the larger HGCN model with six pores (*6*-HGCN), with dihedral angles reaching 50°- 60°. The 2D HGCN nanosheet forms a highly curved layer, analogous to the amorphous form of graphite-like C_3N_4 [23].

Electron density distribution and HOMO-LUMO gap

The electron density distribution in the carbon nitride models is analyzed using the NBO scheme (Figure S1). Particular attention is given to the atomic charges within the nanopore, as these atoms play a major role in gas capture processes. The effect of model size on the charge distribution is also evaluated. All carbon nitride nanopores are composed of alternating negatively charged nitrogen atoms and positively charged carbon atoms. Although the total charge of the nanopores in different carbon nitride models is positive, the interior of each nanopore is negatively charged due to the presence of nitrogen atoms and groups (Figure 3).

Among the studied carbon nitride models, C_3N_3 is the only one with no linker groups between the triazine rings. As a result, C_3N_3 is the carbon nitride with the weakest nucleophilic and electrophilic character of the nitrogens and carbons, respectively. The charges of these atoms from the nanopore are -0.423 and ~0.413 (Figure 3). Therefore, it is expected that the C_3N_3 nanopore will exhibit less selective adsorption among the studied carbon nitrides. The total charge of the nanopore, calculated as the sum of all atomic charges within the pore, is 2.408. The addition of nitrogen groups as a linker group between s-triazine units in PTI leads to an increase in both nucleophilic and electrophilic character of the atoms within the rings. Nitrogen and carbon atoms forming the nanopore are with charges of -0.549 and ~0.625, respectively. The amino groups introduce additional negatively charged centres, with an average group charge of about -0.143. The excess of electron density at these groups is significantly lower than of the other nitrogen atoms. The total nanopore charge in PTI is 3.361, making PTI the model with the highest positive total nanopore charge among the studied systems.

The carbon nitride model with the smallest size of the nanopore, TGCN, possesses the lowest total charge of the nanopore of ~1.665. The carbon atoms in TGCN have a slightly stronger electrophilic character in comparison to those of PTI, while the amino groups are stronger nucleophilic centres with a group charge of about -0.177. The charges of the imine nitrogen atoms forming the nanopore are comparable to those in PTI. This outlines PTI and TGCN as nanopores with centers that provide the strongest adsorption of molecules such as CO_2 and CO, and are expected to have the highest selectivity towards these gases among all the studied structures. In comparison, the HGCN shows a lower excess of electron density on both types of nitrogen centers within the nanopore compared to PTI and TGCN. The total charge of the pore is 2.314.

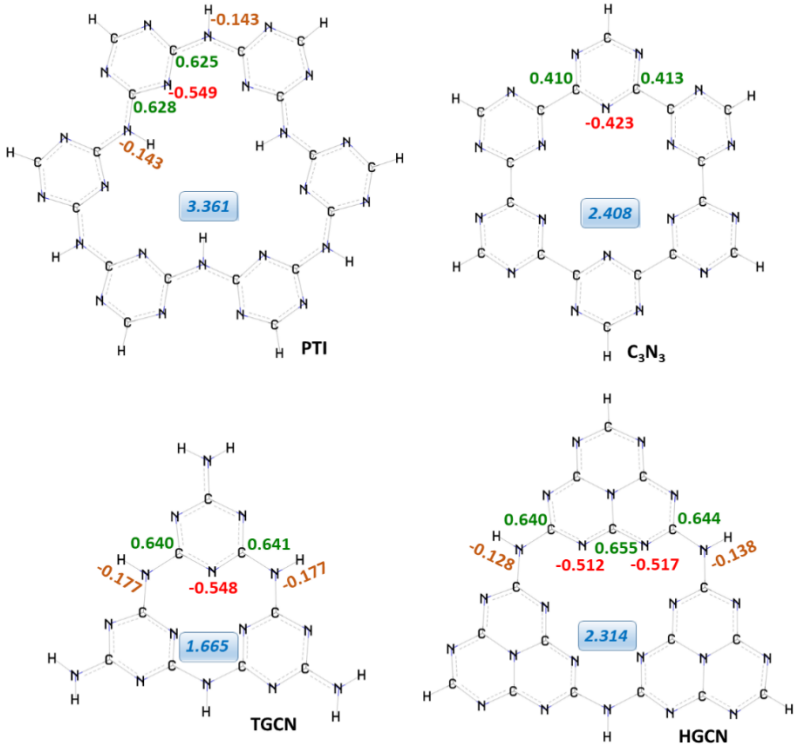

Figure 3. Representative atomic charges of the atoms forming the nanopores in PTI and C_3N_3 (first row); and in TGCN and HGCN nanopore (second row). The charges of carbon atoms are shown in green; of nitrogen atoms in red; total charges of the N-H groups in orange. The total charge of the nanopore is indicated in the blue box.

The trends observed in the charge distribution of the PTI are preserved in the larger model containing ten nanopores (Figure S2). A slight strengthening of the nucleophilic character of the imine nitrogen atoms (atomic charge is -0.565) and the electrophilic character of carbon atoms (atomic charge is 0.637) is observed from the rings participating in more than one cavity. The edge effects are weakly pronounced, manifesting as a minor increase in the absolute charge values of atoms located at the periphery. The central region of the nanosheet displays a slightly higher electron density, suggesting that this part of the layer may be more reactive. Increasing the model size does not affect the total charge of the linking –NH groups. The total charge of the peripheral pores is about 3.380, while the central nanopore is slightly more positive with value of 3.396.

The largest C_3N_3 model (Figure S3) is characterized with a highly homogeneous distribution of the atomic charges within the internal pore. The nitrogen atoms carry of -0.414, while the carbon atoms are charged at 0.414. The excess electron density on the nitrogen atoms is reduced, while the charge of the carbon atoms remains unchanged compared to the smaller C_3N_3 model. The nitrogen atoms at the periphery are the most negatively charged, ranging from -0.454 to -0.457. The total charge of the peripheral nanopores is about 2.462 while the charge of the central nanopore is 2.484.

Similar to the C_3N_3 models, the nucleophilic strength of the imine nitrogens and the electrophilic character of the carbons in the central nanopore decrease from TGCN single-pore model to the nanosheet (Figure S4). There is also a slight disproportionation in the charges of the three imine nitrogens in the central pore: two have charges of -0.518 and -0.512, while the third one has a charge of -0.507. The positive charge on some of the carbons increases to about 0.666. The nitrogens linking three rings reveal a notable excess of electron density, with charges ranging from -0.455 to -0.461, comparable to other nitrogen types in the structure. As a result, the total charge of the central cavity is 1.013, while the charges of the peripheral ones/cavities are around 1.480.

The enlargement of the HGCN (Figure S5) model results in the conversion of the linking -NH groups into nitrogen centres that connect three ring fragments. This structural change leads to an increase in the electron density at these centres, transforming them into much stronger nucleophiles. The larger number of the neighboring nanopores corresponds to a total charge of 1.752 ÷ 1.770, which is significantly smaller than the total charge of 2.314 in the single HGCN nanopore model.

Among the single-pore models, C_3N_3 presents the weakest charge separation between atoms in the nanopore interior, with the smallest absolute charge values. Therefore, it is considered as a slightly less reactive structure in the gas capture process. The addition of -NH linker groups enhance the nucleophilic and electrophilic characters of the atoms in the nanopore of PTI, TGCN, and HGCN. While these three models exhibit relatively similar values of the atomic electron density, TGCN displays the largest absolute charges, suggesting that it is the most reactive structure of the four carbon nitride models. The total nanopore charge decreases in the following order: PTI, C_3N_3, HGCN, TGCN. The charge distribution trends observed in the single-pore models are largely preserved as the model size increases. The most pronounced changes occur in TGCN and HGCN, where nanosheet formation reduces the total nanopore charge due to electron density localization at the linking nitrogen centers. The weak edge effects in all systems suggest potential competition between neighboring nanopores during gas adsorption and separation. Negatively charged nitrogen atoms, especially in the PTI and TGCN nanopores, strongly attract polar and quadrupolar gases such as CO and CO_2, resulting in enhanced adsorption and selectivity in comparison to H_2 and CH_4. H_2 can easily permeate due to its small size and weak interactions with the nanopores.

The dipole moments of the studied carbon nitride models are also considered. PTI and C_3N_3, both in their smaller and larger structures, have no permanent dipole moment. Among the single-pore models, TGCN possesses the largest dipole moment of 1.49 D, followed by HGCN with 0.50 D. The dipole moment values increase significantly as the models enlarge: *10*-TGCN with ten nanopores, doubles its value to 3.03 D, while 6-HGCN with six nanopores increases approximately five times, reaching 5.46 D.

The magnitude of the intrinsic dipole moment in these structures could influence adsorption and selectivity, as well as the transport properties through the nanopores. This could affect their applications as gas separation membranes and photocatalysts.

The energy differences (ΔE, eV) between the lowest unoccupied molecular orbital (LUMO) and the highest occupied molecular orbital (HOMO) for all carbon nitride models are summarized in Table 1. The largest HOMO-LUMO gap is found for PTI (5.24 eV), followed by TGCN (5.01 eV).

Table 1. HOMO-LUMO gap (ΔE in eV) of carbon nitride models, calculated with B3LYP-D3/6-31G**.

	PTI	*10*-PTI	C_3N_3	*7*-C_3N_3	TGCN	*10*-TGCN	HGCN	*6*-HGCN
Δ E, eV	5.24	5.21	3.94	3.79	5.01	4.49	3.65	3.54

Slightly smaller and comparable values are obtained for C_3N_3 and HGCN, 3.94 eV and 3.65 eV, respectively. Enlargement of the structural models does not lead to a meaningful reduction in the energy gap between the two frontier orbitals. C_3N_3 and HGCN with the smaller energy difference, display promising potential for photocatalytic applications, as their band gap can be tuned to enhance light absorption and overall photocatalytic efficiency.

The interaction of these materials with gas molecules can influence the energy levels of the frontier molecular orbitals (HOMO and LUMO), thereby affecting their adsorption properties and selectivity. The large band gap values, particularly for PTI and HGCN, are associated with high chemical stability and low reactivity [24], important characteristics for application of the models as gas separation membranes.

CONCLUSION

A series of carbon nitride models based on s-triazine (PTI, C_3N_3, TGCN) and tri-s-triazine units (HGCN) were studied using density functional theory. The potential of structures with varying nanopore shape and size for use as one-atom thick gas separation membranes was evaluated. Both the smallest single-pore models and the highly porous 2D nanosheets were considered. Increasing the size of the carbon nitride models does not lead to significant structural variations: the PTI nanosheet remains planar and the folding in HGCN is preserved. Edge effects become slightly more pronounced in TGCN, where differences between the central pore and the peripheral ones are observed. As the number of the building units increases, the C_3N_3 nanosheet tends to adopt a more planar structure. Enlargement of the structures is not associated with major redistribution of the electron density, although, a slight increase in the total charge was observed for the central nanopores in the PTI and C_3N_3 nanosheets and a reduction was found for TGCN, and more notable, for HGCN. The relatively similar charge distribution among the nanopores in the nanosheets suggests possible competition between pores during the gas capturing process. The enlargement of the models does not affect the HOMO-LUMO energy difference, indicating good chemical stability of the structures. The studied structural and electronic characteristics of the carbon nitride models are an initial step toward exploring their potential as one atom-thick membranes.

Supporting information: *The following data are provided as Supporting information: atomic charges of the single and multiple-pore models of PTI, C_3N_3, TGCN, HGCN (Figures S1 to S5).*

Acknowledgement: *This work was supported by Project BG16RFPR002-1.014-0006 "National Centre of Excellence Mechatronics and Clean Technologies", co-funded by the European Union, under "Research Innovation and Digitalization for Smart Transformation" program 2021-2027.*

REFERENCES

1. S. Wang, L. Wang, H. Cong, R. Wang, J. Yang, X. Li, Y. Zhao, H. Wang, *J. Environ. Chem. Eng.*, **10**, 108189 (2022).
2. T. Ashirov, J. S. Siena, M. Zhang, A. O. Yazaydin, M. Antonietti, A. Coskun, *Nat. Commun.* **13**, 7299 (2022).
3. S. Hua, D. Qu, L. An, W. Jiang, Y. Wen, X. Wang, Z. Sun, *Appl. Catal. B – Environ*, **240**, 253 (2019).
4. K. Schwinghammer, M. B. Mesch, V. Duppel, C. Ziegler, J. Senker, B. V. Lotsch, *J. Am. Chem Soc.* **136**, 1730 (2014).
5. M. Wu, Q. Wang, Q. Sun, P. Jena, *J. Phys. Chem. C*, **117**, 6055 (2013).
6. X.-L. Zhang, C. Zheng, S. S. Guo, J. Li, H. H. Yang, G. Chen, *Anal. Chem.*, **86**, 3426 (2014).
7. M. Wu, Q. Wang, Q. Sun, P. Jena, *J. Phys. Chem. C.*, **117**, 6055 (2013).
8. G. Dong, Y. Zhang, Q. Pan, J. Qiu, *J. Photochem. Photobiol. C: Photochem. Rev.*, **20**, 33 (2014).
9. Y. Kang, Y. Yang, L. C. Yin, H. M. Cheng, *Adv. Mater.* **27**, 4572 (2015).
10. J. Sehnert, K. Baerwinkel, J. Senker, *J. Phys. Chem.*, **111**, 10671 (2007).
11. Y. Wang, Q. Yang, C. Zhong, J. Li, *J. Phys. Chem. C*, **120**, 28782 (2016).
12. Z. Ma, X. Zhao, Q. Tang, *Int. J. Hydrogen Energy*, **39**, 5037 (2014).
13. B. Zhu, S. Wageh, A. A. Al-Ghamdi, S. Yang, Z. Tian, J. Yu, *Catal. Today*, **335**, 117 (2019).
14. M. T. Vahdat, D. Campi, N. Colonna, N. Marzari, K. V. Agrawal, *J. Phys. Chem. C*, **125**, 18896 (2021).
15. S. W. de Silva, A. Du, W. Senadeera, Y. Gu, *J. Membr. Sci.*, **528**, 201 (2017).
16. Y. Zhou, Y. Wu, H. Wu, J. Xue, H. Wang, *Nat. Commun.*, **13**, 5852 (2022).
17. Y. Ji, H. Dong, H. Lin, L. Zhang, T. Hou, Y. Li, *RSC Adv.*, **6**, 52377 (2016).
18. P. Li, F. Wang, S. Wei, X. Li, Y. Zhou, *Phys. Chem. Chem. Phys.*, **19**, 4405 (2017).
19. J. Wang, Z. Guan, J. Huang, Q. Li, J. Yang, *J. Mater. Chem. A*, **2**, 7960 (2014).

20. S. Grimme, J. Antony, S. Ehrlich, H. Krieg, *J. Chem. Phys.*, **132**, 154104 (2010).
21. A. E. Reed, L. A. Curtiss, F. Weinhold, *Chem. Rev.*, **88**, 899 (1988).
22. M. J. Frisch, G. W. Trucks, H. B. Schlegel, G. E. Scuseria, M. A. Robb, J. R. Cheeseman, G. Scalmani, V. Barone, G. A. Petersson, H. Nakatsuji, X. Li, M. Caricato, A. V. Marenich, J. Bloino, B. G. Janesko, R. Gomperts, B. Mennucci, H. P. Hratchian, J. V. Ortiz, A. F. Izmaylov, J. L. Sonnenberg, D. Williams-Young, F. Ding, F. Lipparini, F. Egidi, J. Goings, B. Peng, A. Petrone, T. Henderson, D. Ranasinghe, V. G. Zakrzewski, J. Gao, N. Rega, G. Zheng, W. Liang, M. Hada, M. Ehara, K. Toyota, R. Fukuda, J. Hasegawa, M. Ishida, T. Nakajima, Y. Honda, O. Kitao, H. Nakai, T. Vreven, K. Throssell, J. A. Montgomery, Jr., J. E. Peralta, F. Ogliaro, M. J. Bearpark, J. J. Heyd, E. N. Brothers, K. N. Kudin, V. N. Staroverov, T. A. Keith, R. Kobayashi, J. Normand, K. Raghavachari, A. P. Rendell, J. C. Burant, S. S. Iyengar, J. Tomasi, M. Cossi, J. M. Millam, M. Klene, C. Adamo, R. Cammi, J. W. Ochterski, R. L. Martin, K. Morokuma, O. Farkas, J. B. Foresman, D. J. Fox, Gaussian, Inc., Wallingford, CT, Gaussian 16, Revision B.01, 2016.
23. J. Sehnert, K. Baerwinkel, J. Senker, *J. Phys. Chem. B*, **111**, 10671 (2007).
24. U. Khan, R. A. Khera, N. Anjum, R. A. Shehzad, S. Iqbal, K. Ayub, J. Iqbal, *RSC Adv.,* **11***,* 7779 (2021).